PERGAMON

International Journal of Solids and Structures 36 (1999) 899–917

INTERNATIONAL JOURNAL OF SOLIDS and STRUCTURES

Development of special finite elements for free boundaries

Ai Kah Soh*

Department of Mechanical Engineering, The University of Hong Kong, Pokfulam Road, Hong Kong

Received 6 August 1997; in revised form 25 October 1997

Abstract

A modified two-dimensional quadrilateral plane stress element and a modified three-dimensional brick element have been developed to eliminate the weakness of the conventional finite elements in determining the stress distributions along free boundaries. The results obtained by the said modified elements are in good agreement with the theoretical and experimental results and are superior to the conventional finite element results. A comparison is made between the proposed approach of improving stress calculations and another approach which employs the least square fitting method. The comparison shows that the two approaches provide comparable accuracy but the latter is more difficult to implement.

1. Notation

x, y, z Cartesian coordinates
n, s, t local Cartesian coordinates with the n axis normal to the boundary
u, v, w displacement components
ξ, η, ζ isoparametric coordinates
σ_x, σ_y, σ_z normal stresses parallel to x, y and z axes, respectively
τ_{xy}, τ_{yz}, τ_{zx} shear stresses in x, y, z coordinates
σ_n, σ_s, σ_t normal stresses parallel to n, s and t axes, respectively
τ_{ns}, τ_{st}, τ_{tn} shear stresses in n, s and t coordinates
σ_ξ, σ_η, σ_ζ normal stresses parallel to ξ, η and ζ axes, respectively
$\tau_{\xi\eta}$, $\tau_{\eta\zeta}$, $\tau_{\zeta\xi}$ shear stresses in ξ, η and ζ coordinates
σ nominal stress

2. Introduction

There are many stress problems which require the determination of the stress distributions along a free boundary with high degree of accuracy. For example, fatigue analysis of offshore tubular

* Tel.: 00852 2858 5415.

0020–7683/99/$ - see front matter
PII: S0020–7683(97)00332–6

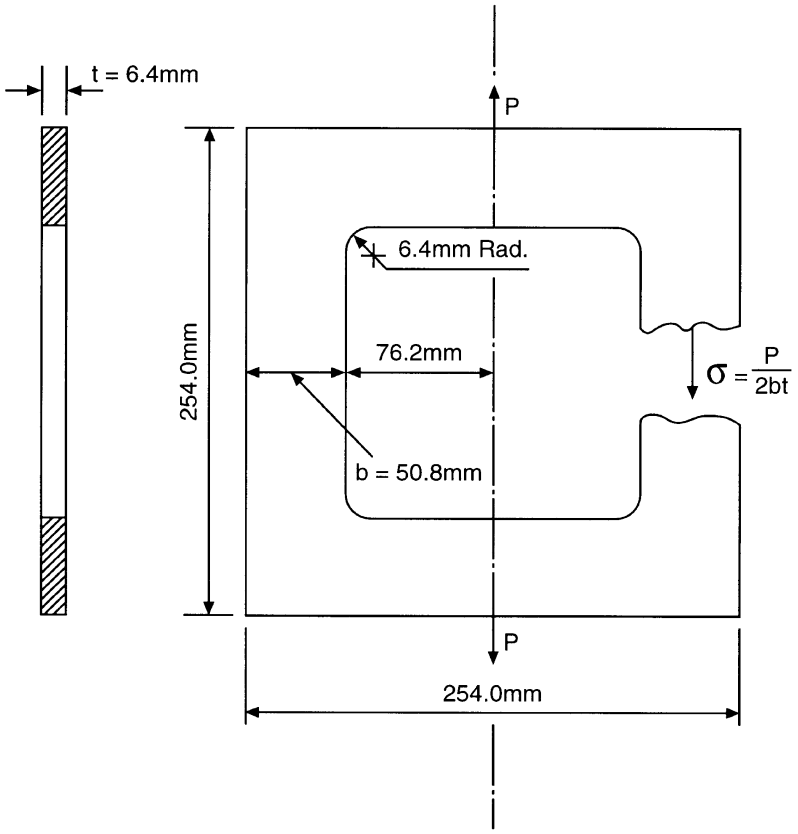

Fig. 1. Portal frame subjected to point loads.

joints are widely performed by the structural engineers who are interested in the hot spot stress, i.e., maximum principal stress, which is the most influential factor affecting the fatigue behaviour of tubular joints. Traditionally, the "hot spot" stresses, which occur at the weld toe of a tubular joint, are determined by extrapolation of stresses on the free surface of the brace or the chord of the joint. Attempts to determine the stress distributions along a free boundary reveal a weakness in the conventional finite element procedure. The weakness of this conventional finite element technique is that, in general, the chosen element displacement functions do not implicitly satisfy the conditions which prevail at a free boundary. As a result, calculations of the boundary stresses based on the element nodal displacements yield non-zero values for the shear and normal stress components, with a corresponding error in the tangential stresses. This is especially marked in the vicinity of geometric stress concentrations, since the boundary stresses can only be determined by extrapolation or some arbitrary means of averaging. Figure 1 shows a portal frame subjected to point loads. The unbalanced stress components have been clearly illustrated by Soh (1992), as reproduced in Fig. 2.

Soh (1992) has proposed a procedure to eliminate the above-mentioned weakness by employing the method of least square fitting. However, the said procedure is tedious because it involves the

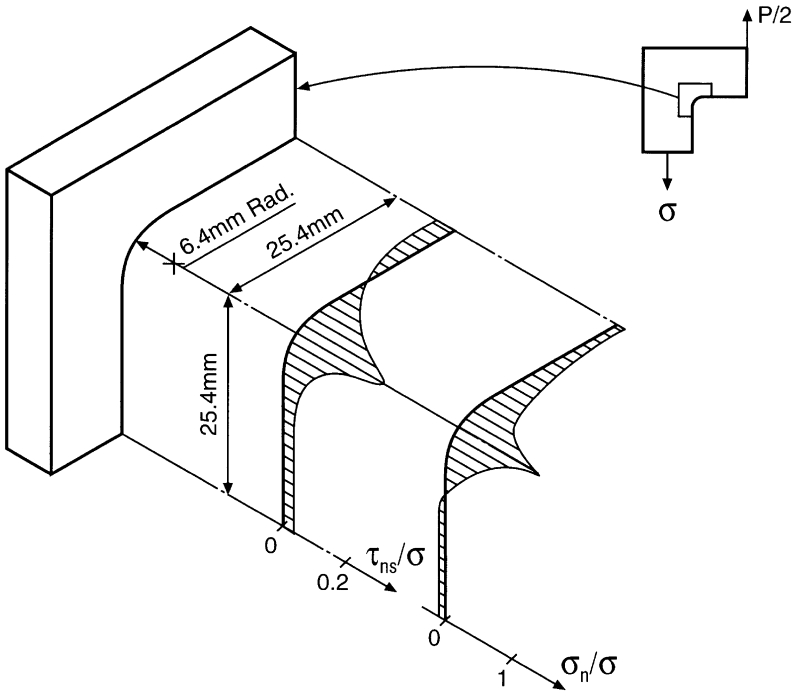

Fig. 2. Unbalanced stress components obtained by the conventional finite element method.

employment of high order polynomials for least square fitting after the determination of all nodal displacements by the conventional finite element method. In this paper, new elements will be developed to eliminate the weakness of the conventional finite element method. The development procedure and potential accuracy of these elements can be illustrated by considering the behaviour of a two- and three-dimensional model subjected to prescribed loads, as shown in Figs 3 and 4, respectively. The corresponding finite element meshes generated are shown in Figs 5 and 6.

3. Analysis

Soh (1992) has proposed that the traditional procedure be used to determine all the nodal displacements without modification. Once the nodal displacements are obtained, new displacement functions, $\{\boldsymbol{f}_f\}$, are fitted by the method of least squares to all the nodes of the elements involved, with the necessary and sufficient conditions imposed to those nodes lying on the free boundary of the elements. Figure 7 shows the 51 nodes involved in least square fitting for determining the stresses at corner node 1 and mid-side nodes 2–5 on a free surface of a three-dimensional body. Note that the necessary and sufficient conditions are implemented at the 21 nodes lying on the free surface. In the case of three-dimensional stress analysis, the assumed displacement functions for least square fitting can be expressed as

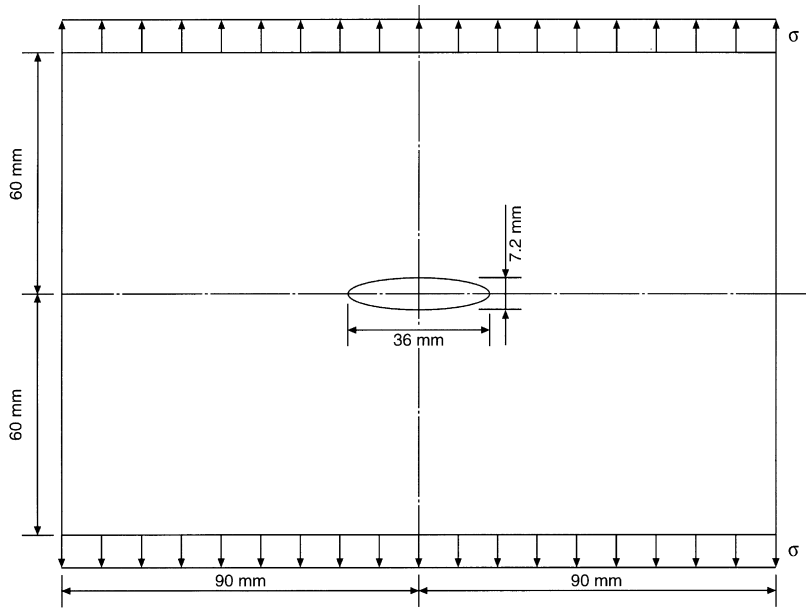

Fig. 3. Rectangular plate with a central elliptic hold subjected to uniform tensile loads.

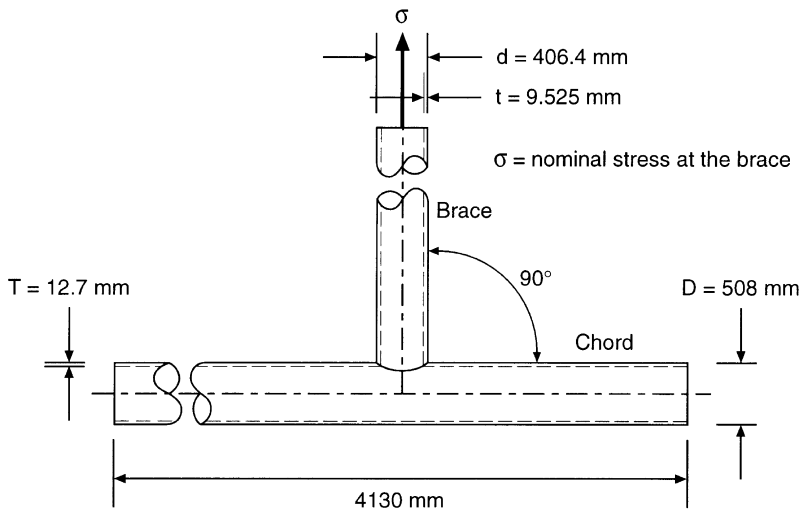

Fig. 4. A T tubular joint subjected to axial load.

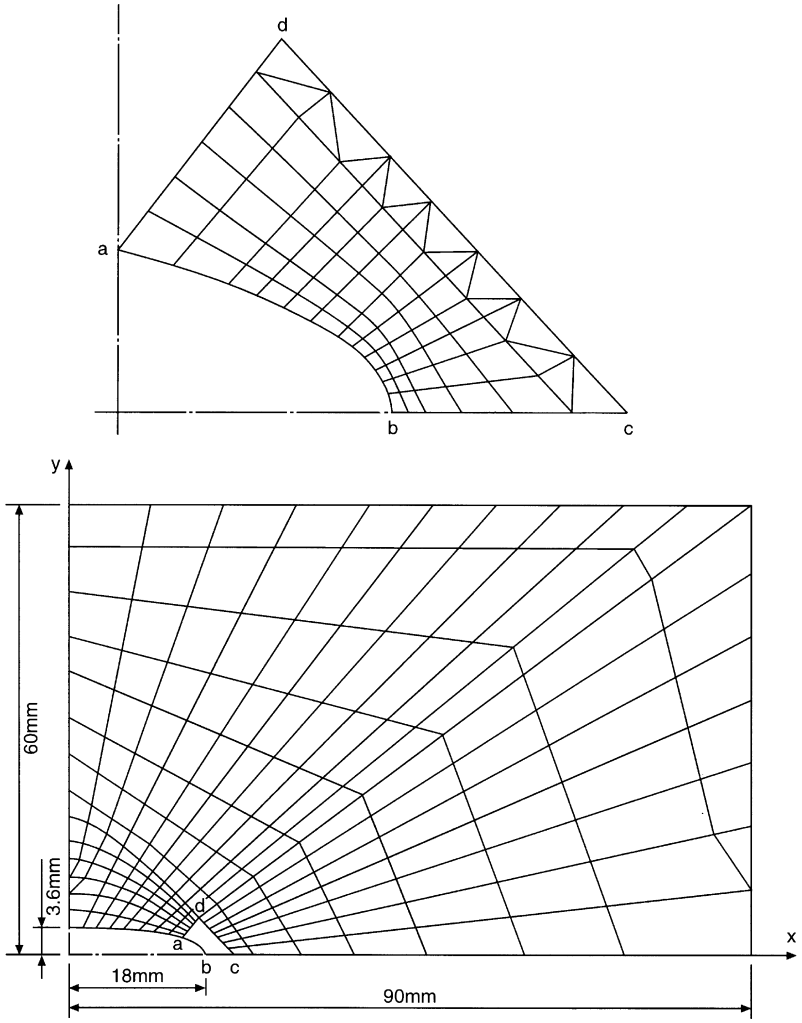

Fig. 5. Mesh generated for two-dimensional finite element analysis.

$$\{\boldsymbol{f}_f\} = [\boldsymbol{\Psi}]\{\mathbf{A}\} \tag{1}$$

where

$$[\boldsymbol{\Psi}] = \begin{bmatrix} \boldsymbol{\psi}(x,y,z) & 0 & 0 \\ 0 & \boldsymbol{\psi}(x,y,z) & 0 \\ 0 & 0 & \boldsymbol{\psi}(x,y,z) \end{bmatrix}$$

and

$$\{\mathbf{A}\} = \{\alpha_1 \quad \alpha_2 \quad \ldots \quad \alpha_n\}^T$$

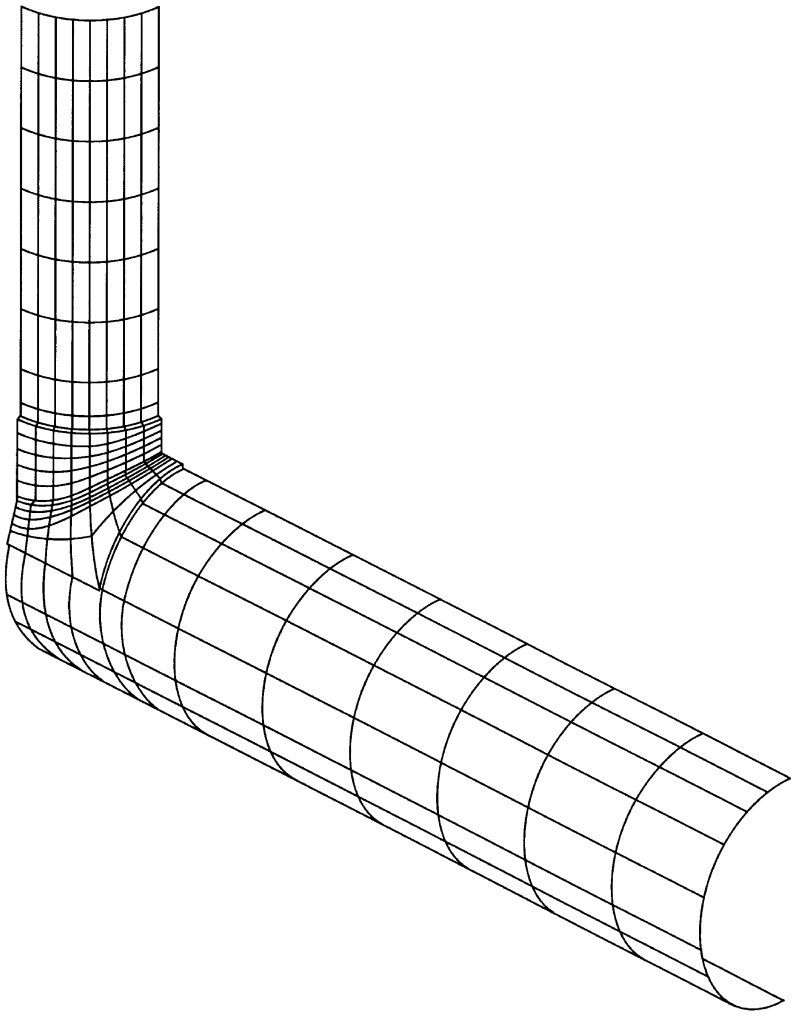

Fig. 6. Finite element mesh for a quarter T joint.

Note that $[\boldsymbol{\psi}(x, y, z)]$ is a row matrix consisting of powers and products of x, y and z; and α_1, $\alpha_2, \ldots, \alpha_n$ are the coefficients of the new displacement functions $\{\boldsymbol{f}_f\}$.

By fitting $\{\boldsymbol{f}_f\}$ to the actual displacements of the 51 nodes involved using the method of least squares, a set of equations can be obtained and expressed as

$$\{\bar{\boldsymbol{d}}\} = \begin{bmatrix} \boldsymbol{\psi}_{cf} & 0 & 0 \\ 0 & \boldsymbol{\psi}_{cf} & 0 \\ 0 & 0 & \boldsymbol{\psi}_{cf} \end{bmatrix} \{\mathbf{A}\} + \{\overline{\boldsymbol{d}_e}\} \tag{2}$$

where $\{\bar{\boldsymbol{d}}\}$ is a column vector consisting of the nodal displacements of the elements involved; $[\boldsymbol{\psi}_{cf}]$

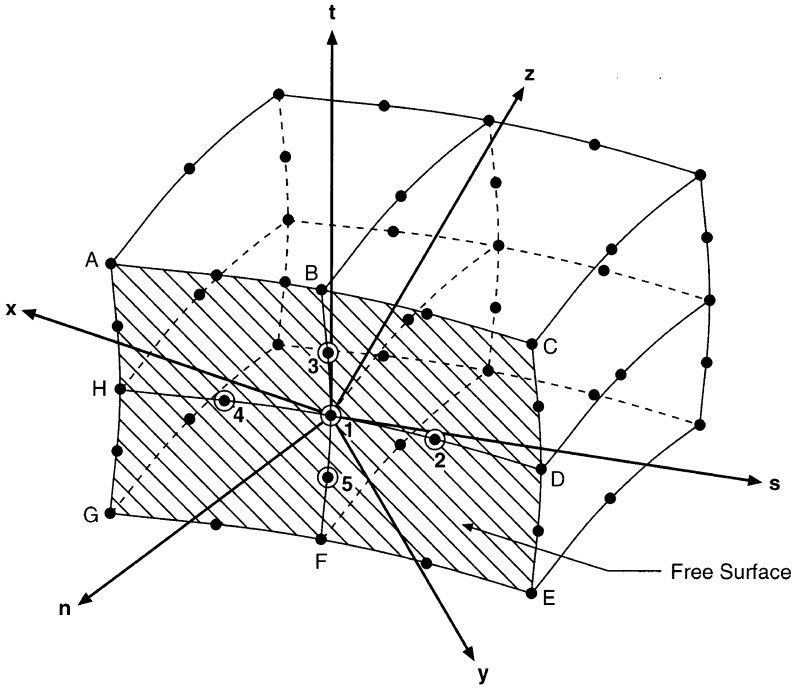

Fig. 7. Nodes involved in least square fitting for determining three-dimensional stresses on a free surface.

is a coefficient sub-matrix consisting of powers and products of x, y, and z; and $\{\overline{\boldsymbol{d}}_e\}$ is a column vector consisting of error terms between the actual and fitted nodal displacements.

The normal stress, σ_n, and the tangential shear stresses, τ_{ns} and τ_{nt}, on the free surface can be expressed as

$$\begin{aligned}\sigma_n &= \phi_1(\alpha_1, \alpha_2, \ldots, \alpha_n, x, y, z) + (\sigma_n)_e \\ \tau_{ns} &= \phi_2(\alpha_1, \alpha_2, \ldots, \alpha_n, x, y, z) + (\tau_{ns})_e \\ \tau_{nt} &= \phi_3(\alpha_1, \alpha_2, \ldots, \alpha_n, x, y, z) + (\tau_{nt})_e \end{aligned} \tag{3}$$

where ϕ_1, ϕ_2 and ϕ_3 are the normal stress, σ_n, and the tangential shear stresses, τ_{ns} and τ_{nt}, respectively, obtained from the assumed displacement functions $\{\boldsymbol{f}_f\}$. $(\sigma_n)_e$, $(\tau_{ns})_e$ and $(\tau_{nt})_e$ are the corresponding error terms.

By setting σ_n, τ_{ns} and τ_{nt} to zero at the 21 nodes lying on the free surface, a set of equations can be obtained. This set of equations can be combined with the set provided by eqn (2), and thus, we obtain

$$\{\boldsymbol{D}\} = [\boldsymbol{\Psi}_c]\{\mathbf{A}\} + \{\boldsymbol{E}\} \tag{4}$$

where $\{\boldsymbol{D}\}$ is a column vector consisting of nodal displacements and zeros; $[\boldsymbol{\Psi}_c]$ is a coefficient matrix consisting of products of x, y and z; and $\{\boldsymbol{E}\}$ is a column vector consisting of the differences between the actual and best fitted displacements/stresses.

$\{\boldsymbol{E}\}^T\{\boldsymbol{E}\}$ should be minimized in order to satisfy the least square condition. Equation (4) can be re-arranged as

$$\{\boldsymbol{E}\} = \{\boldsymbol{D}\} - [\boldsymbol{\Psi}_c]\{\mathbf{A}\}$$

Therefore,

$$\begin{aligned}\{\boldsymbol{E}\}^T\{\boldsymbol{E}\} &= (\{\boldsymbol{D}\}^T - \{\mathbf{A}\}^T[\boldsymbol{\Psi}_c]^T)(\{\boldsymbol{D}\} - [\boldsymbol{\Psi}_c]\{\mathbf{A}\}) \\ &= \{\boldsymbol{D}\}^T\{\boldsymbol{D}\} - 2\{\mathbf{A}\}^T[\boldsymbol{\Psi}_c]^T\{\boldsymbol{D}\} + \{\mathbf{A}\}^T[\boldsymbol{\Psi}_c]^T[\boldsymbol{\Psi}_c]\{\mathbf{A}\}\end{aligned}$$

Setting $\partial(\{\boldsymbol{E}\}^T\{\boldsymbol{E}\})/\partial\{\mathbf{A}\} = 0$ to satisfy the least square condition, then

$$\{\mathbf{A}\} = ([\boldsymbol{\Psi}_c]^T[\boldsymbol{\Psi}_c])^{-1}[\boldsymbol{\Psi}_c]^T\{\boldsymbol{D}\} \tag{5}$$

The best fitted displacement functions obtained can then be used to determine the stress and strain components at the nodes considered by employing the strain–displacement equations and stress–strain relations.

It is obvious that the assumed displacement functions $\{\boldsymbol{f}_f\}$ must be high order polynomials of x, y and z. In the case of three-dimensional stress analysis using 20-noded isoparametric brick elements, the column vector $\{\mathbf{A}\}$ is required to have about 100 coefficients in order to achieve a meaningful least square fitting. Thus, it is not an easy task to determine $([\boldsymbol{\Psi}_c]^T[\boldsymbol{\Psi}_c])^{-1}$ because $[\boldsymbol{\Psi}_c]$ is sizeable. One promising method of achieving the same objective without going through the tedious procedure of least square fitting is to develop new elements with the prevailing conditions at the free boundary implemented.

The displacement functions of a new element can be expressed as

$$\{\boldsymbol{f}\} = [\boldsymbol{N}]\{\boldsymbol{d}\} + \{\boldsymbol{g}\} \tag{6}$$

where

$[\boldsymbol{N}]$ = Element shape function matrix.
$\{\boldsymbol{d}\}$ = Element nodal displacement vector.
$\{\boldsymbol{g}\}$ = Additional displacement vector for implementation of the prevailing conditions at the free boundary.

The prevailing conditions at the free boundary will be implemented on eqn (6) from which the coefficients of the additional displacement functions can be determined. Hence, eqn (6) can be expressed as

$$\{\boldsymbol{f}\} = [\bar{\boldsymbol{N}}]\{\boldsymbol{d}\} \tag{7}$$

where $[\bar{\boldsymbol{N}}]$ is a modified shape function matrix which consists of the original shape functions and the contributions from the additional displacement functions.

The stiffness matrix of the element can be obtained from

$$[\boldsymbol{k}] = \int_{-1}^{1}\int_{-1}^{1}\int_{-1}^{1} [\boldsymbol{B}]^T[\boldsymbol{D}][\boldsymbol{B}] \det[\boldsymbol{J}]\, \mathrm{d}\xi\, \mathrm{d}\eta\, \mathrm{d}\zeta \tag{8}$$

where

$[\boldsymbol{B}]$ = Element strain displacement matrix.

$= [\boldsymbol{L}][\tilde{\boldsymbol{N}}]$

$[\boldsymbol{L}]$ = A suitable linear operator which relates the strain vector, $\{\boldsymbol{\varepsilon}\}$ to the displacement vector, $\{\boldsymbol{f}\}$, of the element.

$[\boldsymbol{D}]$ = Elasticity matrix containing the appropriate material properties.

$\det[\boldsymbol{J}]$ = Determinant of the Jacobian matrix.

This type of element can be employed together with other types of elements to improve the accuracy of the stresses computed at the free boundary.

3.1. *Two-dimensional stress analysis*

Figure 8 shows a typical eight-noded isoparametric element (Bathe, 1996). The displacement components in the element are given by

$$u = \sum_{i=1}^{8} N_i u_i + g_1(\xi, \eta)$$

$$v = \sum_{i=1}^{8} N_i v_i + g_2(\xi, \eta) \tag{9}$$

where

$$N_1 = \frac{1}{4}(1-\xi)(1-\eta) - \frac{N_5}{2} - \frac{N_8}{2}$$

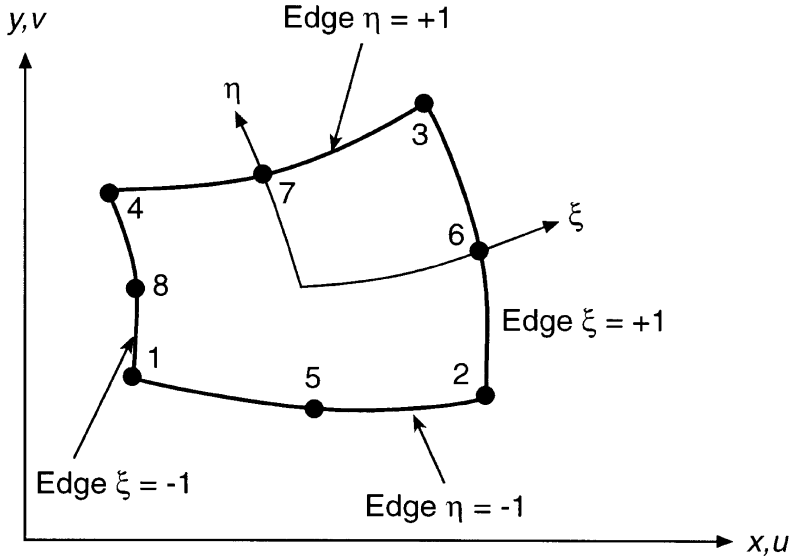

Fig. 8. Eight-noded isoparametric element.

$$N_2 = \frac{1}{4}(1+\xi)(1-\eta) - \frac{N_5}{2} - \frac{N_6}{2}$$

$$N_3 = \frac{1}{4}(1+\xi)(1+\eta) - \frac{N_6}{2} - \frac{N_7}{2}$$

$$N_4 = \frac{1}{4}(1-\xi)(1+\eta) - \frac{N_7}{2} - \frac{N_8}{2}$$

$$N_5 = \tfrac{1}{2}(1-\xi^2)(1-\eta)$$

$$N_6 = \tfrac{1}{2}(1+\xi)(1-\eta^2)$$

$$N_7 = \tfrac{1}{2}(1-\xi^2)(1+\eta)$$

$$N_8 = \tfrac{1}{2}(1-\xi)(1-\eta^2) \tag{10}$$

and u_i and v_i are nodal displacement components in the ξ and η directions, respectively. The functions g_1 and g_2 are to be assumed based on the compatibility conditions that prevail at the boundaries of the element. In the case where one of the four edges of the element, say $\eta = 1$, is a free boundary, the said functions can be assumed to be

$$g_j(\xi,\eta) = C_{j1}(1-\xi^2)(1-\eta^2) + C_{j2}\xi^2(1-\xi^2) + C_{j3}\eta^2(1-\eta^2) \tag{11}$$

where $j = 1, 2$ and $C_{11}, C_{12}, \ldots, C_{23}$ are arbitrary constants.

Since the normal stress, σ_η, and the tangential shear stress, $\tau_{\eta\xi}$, along the free boundary are zero, these two conditions are to be imposed on each of the nodes lying on the free boundary. With reference to Fig. 8, it can be shown that

$$\sigma_\eta = \frac{E}{(1-v^2)}\left[\frac{\partial v}{\partial \eta} + v\frac{\partial u}{\partial \xi}\right]$$

$$\tau_{\eta\xi} = G\left(\frac{\partial u}{\partial \eta} + \frac{\partial v}{\partial \xi}\right) \tag{12}$$

where E and v are the modulus of elasticity and Poisson's ratio of the material, respectively.

By implementing these two conditions at the three nodes lying on the free edge, the six arbitrary constants can be determined, i.e.,

$$C_{11} = \tfrac{1}{8}[u_1 + u_2 - u_3 - u_4 - 2u_5 + 2u_7]$$

$$C_{12} = \frac{1}{8}\left\{4(u_3+u_4) - 8u_7 + \frac{1}{v}[v_2 - v_1 + 3(v_3 - v_4) - 4(v_6 - v_8)]\right\}$$

$$C_{13} = \tfrac{1}{8}[u_1 + u_2 + 3(u_3+u_4) - 4(u_6+u_8) + 2(v_3 - v_4)]$$

$$C_{21} = \tfrac{1}{8}[v_1 + v_2 - (v_3+v_4) - 2(v_5 - v_7)]$$

$$C_{22} = \tfrac{1}{8}[-u_1 + u_2 + 3(u_3 - u_4) - 4(u_6 - u_8) + 4(v_3+v_4) - 8v_7]$$

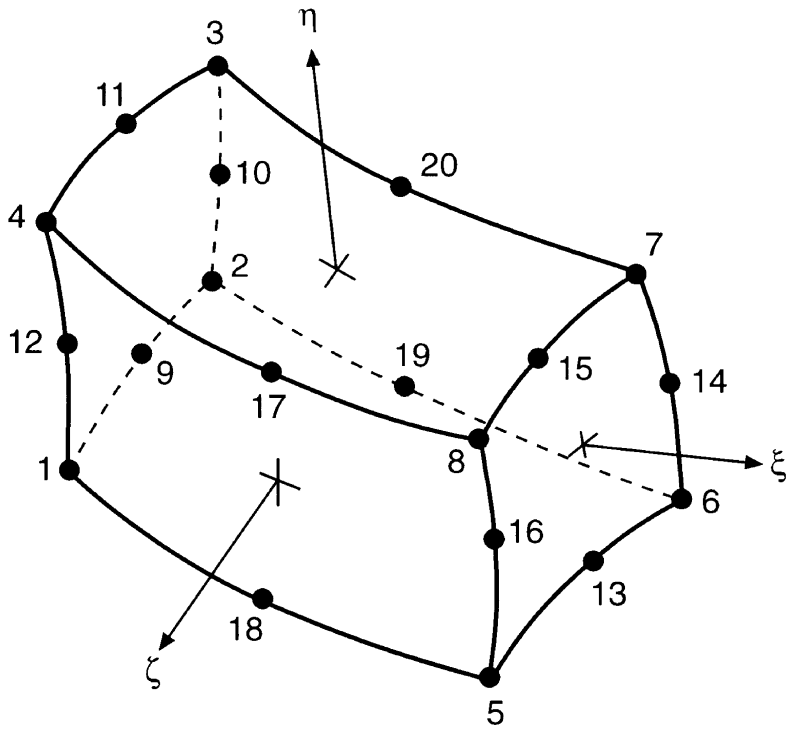

Fig. 9. Twenty-noded isoparametric element.

$$C_{23} = \tfrac{1}{8}[v_1 + v_2 + 3(v_3 + v_4) - 4(v_6 + v_8) + 2v(u_3 - u_4)]$$

Thus, $[\bar{\boldsymbol{N}}]$ can be established and the element stiffness matrix, $[\boldsymbol{k}]$ can be developed.

With reference to Fig. 5, all the elements with a free boundary at the elliptic hole are of the proposed element type and the rest of the elements are the traditional eight-noded isoparametric quadrilateral elements.

3.2. *Three-dimensional stress analysis*

Figure 9 shows a typical 20-noded isoparametric element (Bathe, 1996). The displacement components in the element are given by

$$u = \sum_{i=1}^{20} N_i u_i + g_1(\xi, \eta, \zeta)$$

$$v = \sum_{i=1}^{20} N_i v_i + g_2(\xi, \eta, \zeta)$$

$$w = \sum_{i=1}^{20} N_i w_i + g_3(\xi, \eta, \zeta) \tag{13}$$

where

$$N_j = \tfrac{1}{4}(1-\xi^2)(1+\eta\eta_j)(1+\zeta\zeta_j) \quad \text{for } j = 17, 18, 19, 20 \tag{14}$$

$$N_k = \tfrac{1}{4}(1+\xi\xi_k)(1-\eta^2)(1+\zeta\zeta_k) \quad \text{for } k = 10, 12, 14, 16 \tag{15}$$

$$N_l = \tfrac{1}{4}(1+\xi\xi_l)(1+\eta\eta_l)(1-\zeta^2) \quad \text{for } l = 9, 11, 13, 15 \tag{16}$$

$$N_i = \tfrac{1}{8}(1+\xi\xi_i)(1+\eta\eta_i)(1+\zeta\zeta_i) - \tfrac{1}{2}(N_j + N_k + N_l) \quad \text{for } i = 1, 2, \ldots, 8 \tag{17}$$

Note that $(N_j+N_k+N_l)/2$ refers to only the three nodes adjacent to node i; and ξ_i, η_i, $\zeta_i = \pm 1$.

w_i are the nodal displacement components in the ζ direction; and the functions g_1, g_2 and g_3 can be assumed to be

$$\begin{aligned} g_k(\xi,\eta,\zeta) &= C_{k1}(1-\xi^2)(1-\eta^2) + C_{k2}(1-\eta^2)(1-\zeta^2) + C_{k3}(1-\zeta^2)(1-\xi^2) \\ &+ C_{k4}\eta^2\zeta(1-\xi^2) + C_{k5}\eta\zeta^2(1-\xi^2) + C_{k6}\zeta^2\xi(1-\eta^2) \\ &+ C_{k7}\zeta\xi^2(1-\eta^2) + C_{k8}\xi^2(1-\zeta^2) + C_{k9}\xi\eta^2(1-\zeta^2) \end{aligned} \tag{18}$$

where $k = 1$, 2 and 3 and C_{11}, $C_{12}, \ldots, C_{39}$ are arbitrary constants.

Since the two tangential shear stress, $\tau_{\eta\xi}$ and $\tau_{\eta\zeta}$, and the normal stress, σ_η, on the free surface situated at $\eta = 1$ are zero, these three conditions are to be imposed on each of the nodes lying on the free surface. Moreover, the said conditions are imposed at the centre of the free surface so that the additional displacement functions selected have the right number of terms to give equal weighting to all three directions, ξ, η and ζ. With reference to Fig. 9, it can be shown that

$$\begin{aligned} \sigma_\eta &= \frac{E(1-v)}{(1-2v)(1+v)}\left[\frac{\partial v}{\partial \eta} + \frac{v}{(1-v)}\left(\frac{\partial u}{\partial \xi} + \frac{\partial w}{\partial \zeta}\right)\right] \\ \tau_{\eta\xi} &= G\left(\frac{\partial u}{\partial \eta} + \frac{\partial v}{\partial \xi}\right) \\ \tau_{\eta\zeta} &= G\left(\frac{\partial w}{\partial \eta} + \frac{\partial v}{\partial \zeta}\right) \end{aligned} \tag{19}$$

By implementing these three conditions at the eight nodes and the centre point lying on the free surface, the 27 arbitrary constants can be expressed in terms of the nodal displacements of the elements. Thus, $[\bar{\boldsymbol{N}}]$ can be established and the element stiffness matrix, $[\boldsymbol{k}]$ can be developed.

With reference to Fig. 6, all the brick elements are of the proposed element type and the rest of the elements are eight-noded shell elements (Bathe, 1996).

3.3. *The conventional method*

One of the most commonly used methods for determining the stress components at a nodal point lying on a free boundary is the graphical extrapolation method. This method uses the values of the stresses obtained for internal elements in the vicinity of the boundary node being considered. The method can be easily illustrated by considering a two-dimensional problem, as shown in

Fig. 10. For the data presented in the figure, six nodal points have been used in making extrapolations to determine σ_x, σ_y and τ_{xy} at each corner node along the free boundary of the structure. Note that the values of σ_x, σ_y and τ_{xy} at each of the six nodal points are obtained by averaging the corresponding nodal stresses of those elements sharing the said nodal point. However, in the case of mid-side node only five nodal points were used in making extrapolations. The values of σ_n, σ_s and τ_{ns} are then determined using the Mohr circle at points where the normal to the boundary does not coincide with either the x or y axis.

The procedure is also applicable to three-dimensional problems. However, the said procedure needs modification for the analysis of the present three-dimensional model due to the fact that there are only two layers of solid elements through the thickness of the brace and chord (refer to Fig. 6). In the present case, the hot spot stresses, i.e., maximum principal stresses, which occur at the brace/chord intersection, are determined using both the averaging and graphical extrapolation methods. Note that the former evaluates the stress components at a surface node by taking the average of the corresponding components at the surrounding Gauss points. For the data presented in Fig. 11, only two nodal points have been used, in order to be consistent with the experimental procedure recommended by the U.K. Department of Energy Guidance Notes (1982), in making extrapolations to determine σ_x, σ_y, σ_z, τ_{yz}, τ_{zx} and τ_{xy} at each node lying on the weld toe of the chord side. Note that the values of σ_x, σ_y, σ_z, τ_{yz}, τ_{zx} and τ_{xy} at each of the two nodal points are obtained by averaging the corresponding stress components of the surrounding Gauss points. The hot spot stress at the nodal point considered can then be determined by transformation of stresses.

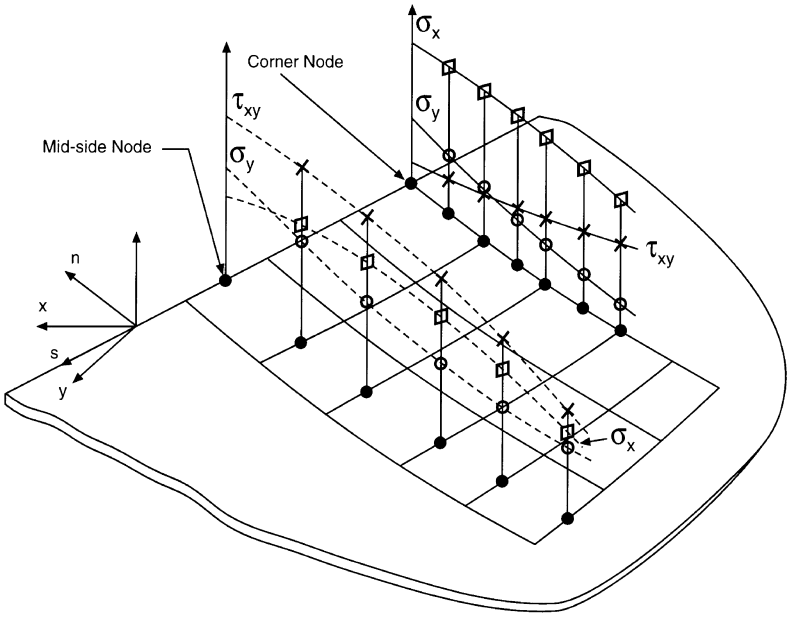

Fig. 10. Two-dimensional stress components obtained at boundary by extrapolation.

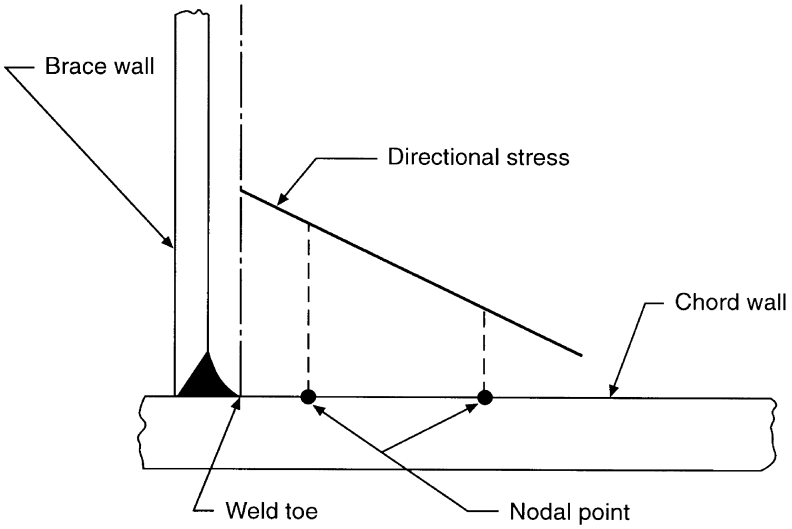

Fig. 11. Extrapolation of directional stress to the weld toe of the chord side for the three-dimensional analysis.

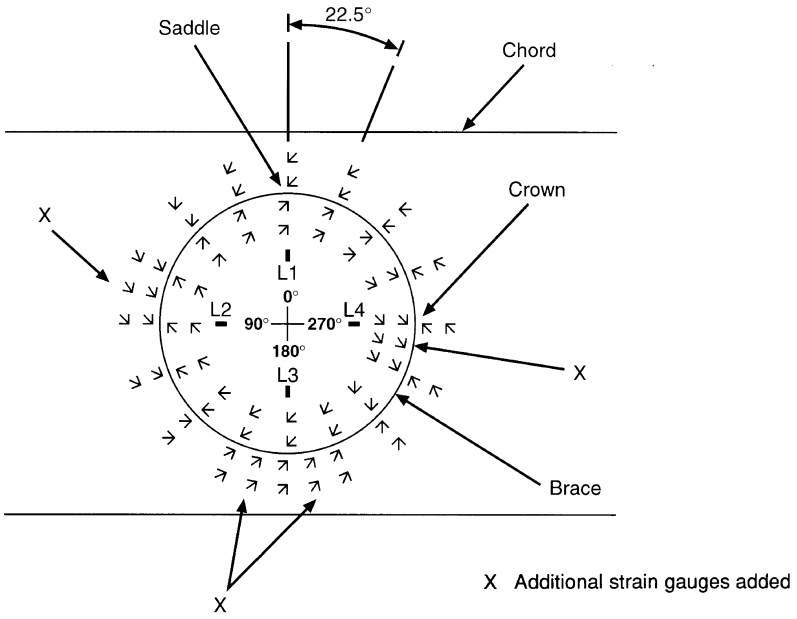

Fig. 12. Strain gauging plan.

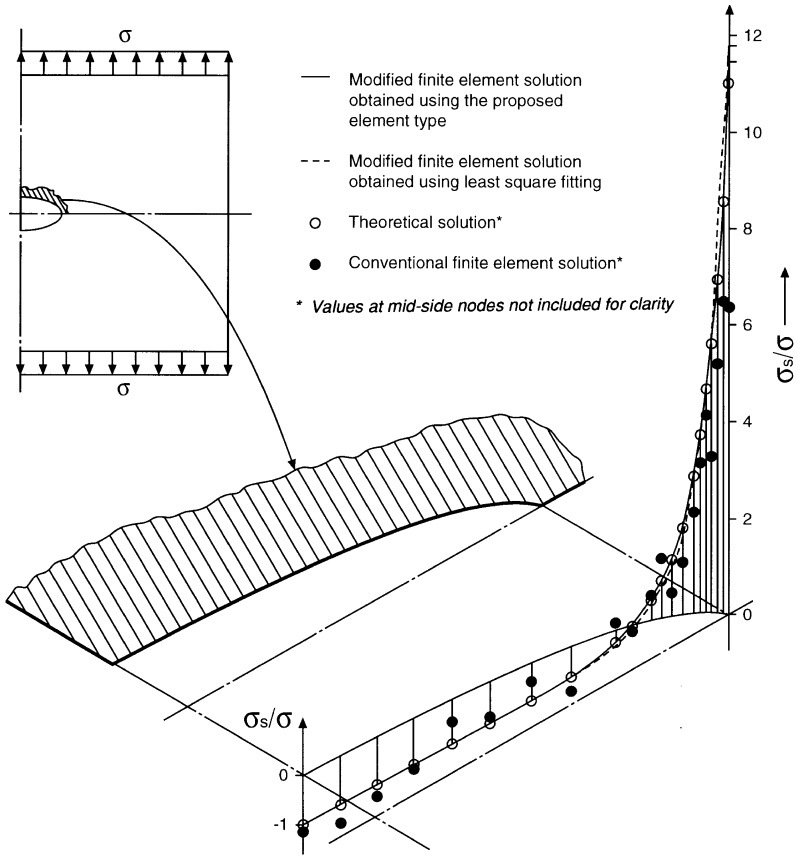

Fig. 13. Comparison of the theoretical and finite element solutions for a two-dimensional model.

4. Experimental test

A steel specimen (Fig. 4) was strain gauged as per the recommendations of the U.K. Department of Energy Guidance Notes (1982). The strain gauges (Dally and Riley, 1991) were placed around the whole brace/chord intersection on both brace and chord at 22.5° intervals, with additional strain gauges being added to confirm some trends. Gauges were placed on the outside surface of both brace and chord. A plan view of the layout is shown in Fig. 12. Note that the gauges on the brace are shown inside the brace diameter. Three-element rectangular rosettes with 2 mm gauge length were used for all strain measurements to enable calculation of principal stresses. The strain gauges measure strain caused by membrane and bending effects which occur on the outside surface where the peak stresses were expected.

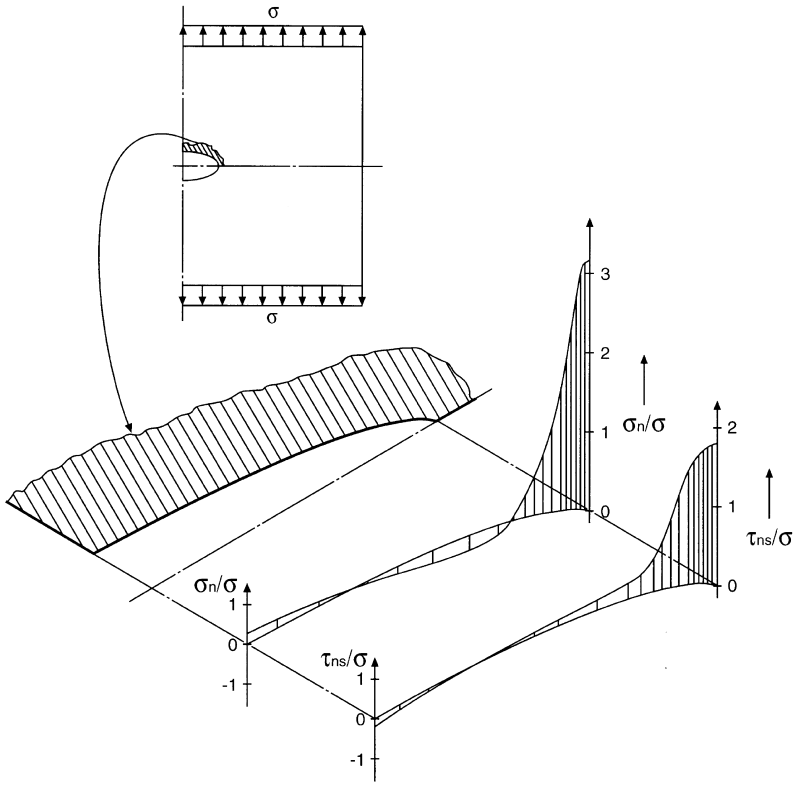

Fig. 14. Unbalanced stress components obtained by the conventional finite element method.

5. Discussion of results

5.1. *Two-dimensional stress analysis*

Figure 13 shows that the two modified finite element solutions, one obtained using the proposed element type and the other using the least square fitting method, are in good agreement with the theoretical solution. Moreover, the said modified solutions are superior to the conventional finite element solution. The maximum normalized tangential normal stress, $(\sigma_s/\sigma)_{\max}$, obtained by the former and latter modified methods are 11.4 and 11.8, respectively. This is close to the corresponding theoretical value of 11.0. However, the corresponding value obtained by the conventional finite element method is only 6.5 which occurs at a location slightly away from that of the other three solutions.

The improvements made by the use of the modified element type and analysis procedure are entirely due to the imposition of the correct free boundary conditions by setting σ_n and τ_{ns} to zero. It is a salutary experience to observe the magnitude of the unbalanced stress components, as shown in Fig. 14, which are yielded by the conventional finite element method. The high values of σ_n and

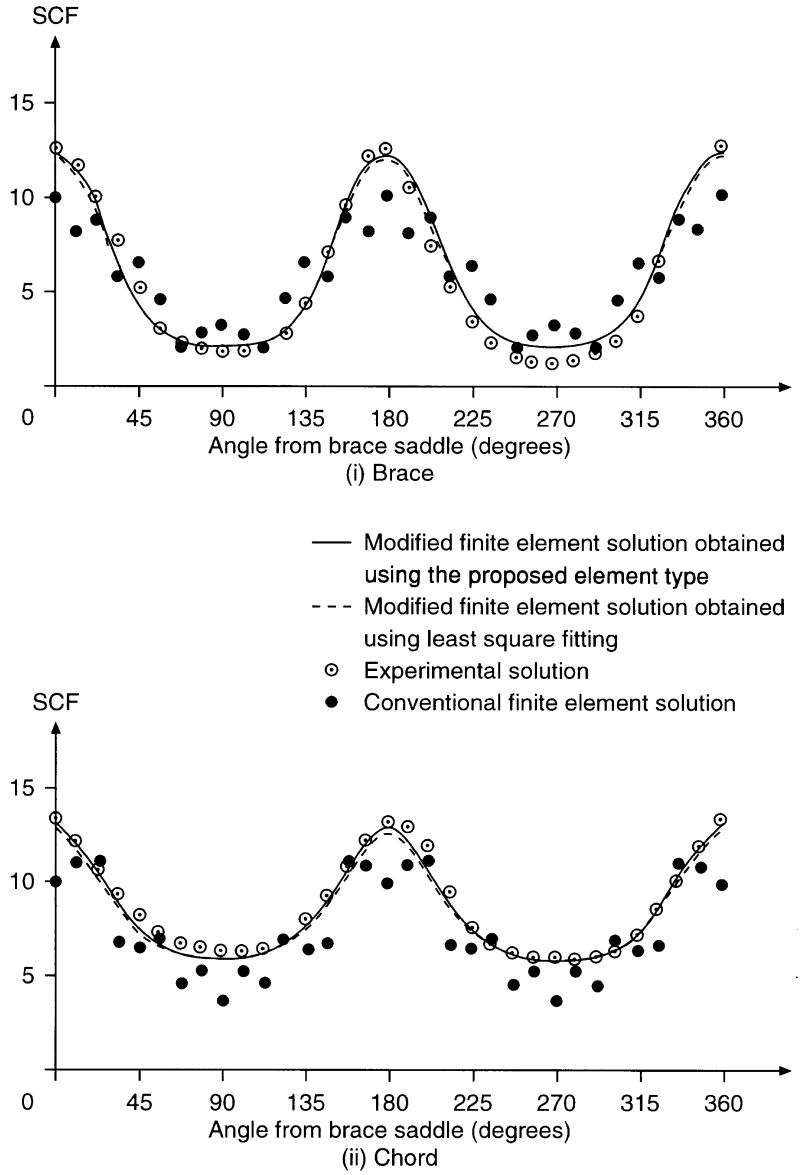

Fig. 15. Stress distributions along the brace/chord intersection of a T joint subjected to axial load.

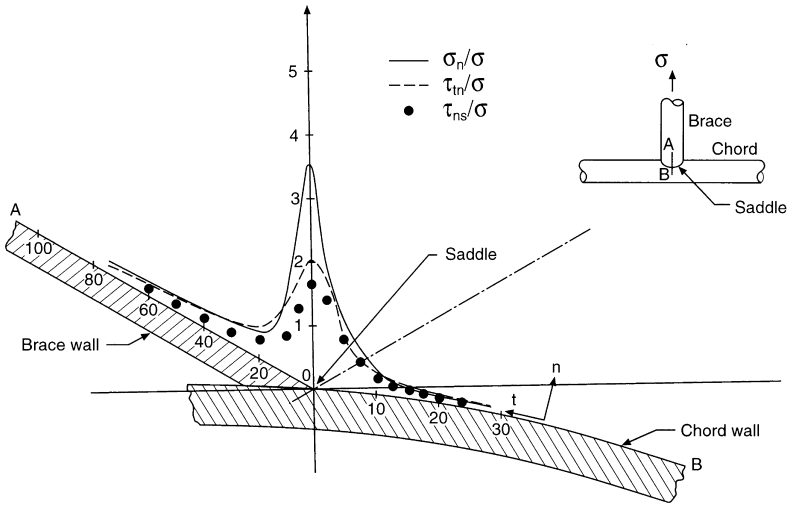

Fig. 16. Unbalanced stress components obtained by the conventional finite element method.

τ_{ns} developed around the major axis of the elliptic hole provide an adequate explanation for the error observed in the tangential boundary stress when this is calculated by the conventional method.

5.2. *Three-dimensional stress analysis*

Figure 15 shows the distributions of the stress concentration factor (hereafter called SCF), which is defined as the ratio of the hot spot stress to the nominal stress at the brace, obtained by the finite element and experimental techniques, for the tubular joint subjected to an axial load. Both the modified finite element solutions and the experimental results are in good agreement and the results are superior to the conventional finite element solution, especially in the region where high stress concentrations occur.

The improvements made by the use of the modified element type and analysis procedure are again entirely due to the imposition of the correct free boundary conditions by setting σ_n, τ_{ns} and τ_{tn} to zero. The high values of σ_n, τ_{ns} and τ_{tn} developed near the weld toe of the tubular joint, as shown in Fig. 16, provide an adequate explanation for the error observed in the hot spot stress, as indicated by the SCF, when this is calculated by the conventional method.

6. Conclusions

The reliability and potential accuracy of the proposed element types for determining free boundary stress distributions in two- and three-dimensional problems have been clearly illustrated. It is worth noting that although the modified analysis procedure can provide comparable accuracy in determining free boundary stresses, the tedious procedure of least square fitting can be avoided

by employing the proposed element types. Moreover, the proposed approach for modifying finite elements is not confined to two-dimensional quadrilateral and three-dimensional brick elements, but is equally applicable to all other element configurations with only minor or no modifications to the proposed approach.

References

Bathe, K. J. (1996) Formulation and calculation of isoparametric finite element matrices. *Finite Element Procedures*, pp. 338–484. Prentice-Hall, Englewood Cliffs, NJ.

Dally, J. W. and Riley, W. F. (1991) Electrical-resistance strain gages. *Experimental Stress Analysis*, pp. 164–213. McGraw-Hill, Singapore.

Department of Energy (1982) Background to new fatigue design guidance for steel welded joints in offshore structures. Report of energy guidance notes revision drafting panel, pp. 37–58. HMSO, London.

Soh, A. K. (1992) An improved method for determining free boundary stresses. *Journal of Strain Analysis* **27**(2), 93–99.